Direct numerical simulation of the early development of a turbulent mixing layer downstream of a splitter plate

Neil D. Sandham [a*] and Richard D. Sandberg[a]

[a]*Aerodynamics and Flight Mechanics Research Group, School of Engineering Sciences, University of Southampton, Southampton SO17 1BJ, UK*;

(*2008*)

A direct numerical simulation is carried out of the initial stages of development of a mixing layer with a velocity ratio of ten, a fast stream Mach number of 0.6 and equal free-stream temperatures. The fast stream is a fully-developed turbulent boundary layer with a trailing-edge displacement thickness Reynolds number of 2300, while the slow stream is laminar. The computations include a splitter plate with zero thickness. The initial flow development is dominated by the rapid spreading of an internal shear layer formed as the viscous sub-layer of the upstream turbulent boundary layer crosses the trailing edge. A tendency towards spanwise-coherent structures is observed very early in the shear layer development, within five displacement thicknesses of the trailing edge, despite such structures not being present in the upstream boundary layer. A numerical search for a global mode in the vicinity of the splitter plate trailing edge found only convective growth of disturbances. Instead, a convective mechanism is examined and found to be a plausible explanation for the rapid change of observed flow structure near the trailing edge. The same mechanism indicates a trend towards more two-dimensional structures in the fully-developed mixing layer.

Keywords: DNS; Mixing layer; compressible; coherent structure; trailing edge; splitter plate

1. Introduction

The experiments of Brown & Roshko [1] can be said to have initiated a new era of research in turbulence, emphasising the role of coherent structures, that continues to the present day. Their experiments illustrated the development of large-scale spanwise-coherent rollers. Importantly these structures did not disappear as the Reynolds number increased and thus could not be easily dismissed as a transitional or low-Reynolds-number phenomenon. The structures are clearly active in entraining fluid, and significant effort has been devoted to understanding their role in mixing and combustion applications (e.g. Broadwell & Mungal [2]). Despite a large body of subsequent research, a convincing explanation of the origin of the striking two-dimensionality of Brown-Roshko structures is still elusive. In particular, the temporally-developing mixing layer direct numerical simulations (DNS) of Rogers & Moser [3] only showed clear Brown-Roshko structures when additional two-dimensional forcing was included in the initial condition.

The review by Ho & Huerre [4] covers a number of mechanisms that are active in free shear layers and may contribute to the formation of coherent structures. These include linear and nonlinear stability, vortex dynamics, global feedback and trailing-edge receptivity. An explanation based on linear stability theory would be

---

*Corresponding author. Email: n.sandham@soton.ac.uk

that the primary inviscid instability is most unstable as a two-dimensional disturbance and hence the mixing layer, which is convectively unstable, will naturally tend to amplify such structures in preference to oblique waves. However, when one looks closer at the amplification rate curves as a function of wave angle it is clear that the curves are almost flat for angles near zero degrees. With random forcing one would expect to find evidence for some structures with significant obliqueness. Instead the experiments are dominated by structures at zero degrees.

The subject has re-emerged recently since the latest direct numerical simulations of subsonic temporally-developing mixing layers are rather notable for the absence of Brown-Roshko structures. Neither the inert low Mach number simulation of Mathew et al. [5] nor the incompressible simulations of Tanahashi et al. [6] show clear organised structure. Such simulations might appear to support the stability argument that, although two-dimensional waves are most unstable, there is a band of unstable oblique waves that are also strongly unstable and that will break down nonlinearly into turbulence without spanwise coherence. This is important because Mathew et al. found that entrainment proceeded more by the old idea of 'nibbling' (small turbulence eddies entraining fluid at the edge of the turbulent region), rather than by 'engulfment' of large lumps of unmixed fluid into the centre of the shear layer, as would be the case if Brown-Roshko structures are active. One possible (though controversial) explanation would be that the Brown-Roshko structures are an artifact of the experiments, for example via the influence of upstream conditions or the constraining presence of sidewalls. If this were the case the temporally-developing simulations might be more representative of mixing processes in some practical applications.

Other explanations for the presence of spanwise-coherent structures focus on the presence of a splitter plate in the experiments. This has two interesting consequences. Firstly there will be a small wake behind the trailing edge (documented experimentally by Mehta [7]) and such wakes may be absolutely unstable. The presence of a spanwise-coherent resonator due to such an instability may lead to spanwise coherency, although this may only happen for thick splitter plates, as in Lee & Morris [8]. Secondly, the trailing edge of the splitter plate is a spanwise line and a receptivity process (Barone & Lele [9]) along that line might provide a bias towards two-dimensional structures, at the expense of oblique modes. Such a receptivity mechanism is only poorly understood at present, and suggests the need for simulations that include the trailing edge itself. Spatially-developing simulations with prescribed inflow conditions downstream of the trailing edge may not be enough to reproduce the experiments (unless the inflow boundary condition inadvertently mimics the receptivity mechanism) and it is only recently that large DNS including the splitter plate have become feasible. One previous simulation of a subsonic mixing layer that includes a trailing edge is due to Laizet & Lambellais [10], who considered the differences between a bevelled and blunt trailing edge, finding a self-excited near wake for the latter configuration.

In the present contribution we modify the trailing-edge aeroacoustics simulation of Sandberg & Sandham [11] to study the initial development of the mixing layer formed after an infinitely thin trailing edge. A structure parameter is used to quantify the change in the flow from more streamwise-oriented structures in the turbulent boundary layer upstream of the trailing edge to more spanwise-coherent structures immediately downstream of the trailing edge. Results are interpreted in the light of the above discussion.
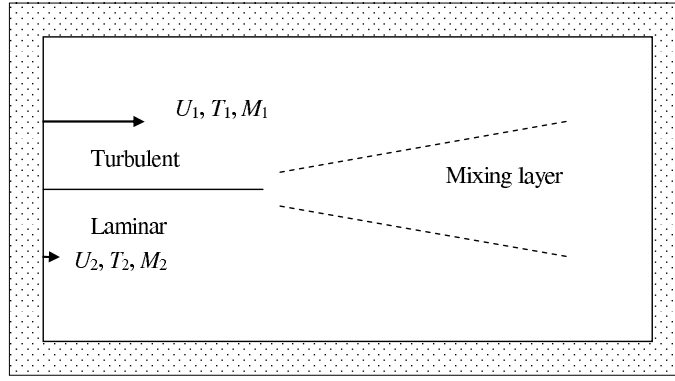
Figure 1.   Schematic of the computational arrangement, with a mixing layer developing from two boundary layers either side of a splitter plate. The shaded area indicates the sponge and zonal characteristic regions that surround the domain of interest.

2.   Methodology

The code used for the present study employs fourth order accurate finite differences in space and a fourth order Runge-Kutta time advance with entropy splitting and other conditioning of the compressible Navier-Stokes equations (Yee et al.[12]; Sandham et al.[13]). When run as a direct numerical simulation the code does not use upwinding, filtering or additional dissipation. The code has previously been validated for various test cases including compressible turbulent channel flow and Tollmien-Schlichting wave growth and has been recently applied to a turbulent wake flow (Sandberg & Sandham [11]) and to flow over a NACA0012 aerofoil (Jones et al.[14]).

Figure 1 shows the general arrangement for the present simulation. An upper stream with velocity $U_1 = 1$, Mach number $M_1 = 0.6$ and temperature $T_1 = 1$ is mixed with a lower stream with velocity $U_2 = 0.1$, $M_2 = 0.06$ and temperature $T_2 = 1$. A high velocity ratio configuration was chosen due to the limited computational data in this flow regime. The upper stream is turbulent while the lower stream is laminar. Initially an arbitrary length scale is specified and, after the simulation has run, all lengths are re-normalised with the displacement thickness of the turbulent boundary layer at the trailing edge so that $\delta^*_{TE} = 1$. In these scaled co-ordinates the computational domain extends for $-113.3 < x < 200.5$, $-113.3 < y < 113.3$ and $0 < z < 17.44$ in the streamwise, lateral and spanwise directions respectively. The trailing edge of the splitter plate is located at $x = 0, y = 0$. At the trailing edge the displacement thickness of the laminar boundary layer on the lower surface is 0.38.

Inflow conditions for the fast stream are based on a synthetic turbulence approach, details of which are given in [11], together with the numerical treatment applied at the trailing edge point and its validation against triple deck theory. With regard to the inflow turbulence, it is important to note that no two-dimensional forcing modes are included. A zonal characteristic boundary condition (Sandberg & Sandham [15]) is applied at the outflow plane. At the lateral boundaries a sponge zone is used. Periodic boundary conditions are applied in the spanwise direction.

The simulation uses a computational grid of $4001 \times 513 \times 225$, giving a total of 462 million grid points and was run on 2048 processors of the UK national high performance computer facility HECToR. The grid is stretched in both the streamwise and lateral directions so that more points are concentrated near the splitter plate (stretching in y) and at the trailing edge (stretching in x). The simulation has been run up to a dimensionless time $t = 502$ (using δ^*_{TE}/U_1 as the reference timescale). This is sufficient for a starting vortex travelling at $U_c = (U_1 + U_2)/2$
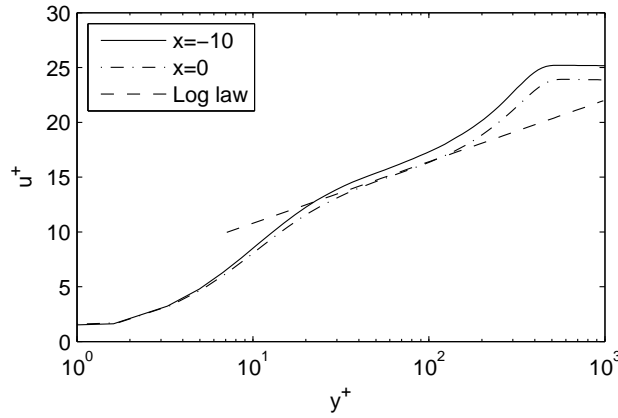
Figure 2.   Mean streamwise velocity profiles in the turbulent boundary layer upstream and at the trailing edge. The log law shown on the figure is taken as $u^+ = 1/0.41 \ln y^+ + 5.17$

to travel through the complete domain, but is not long enough to collect reliable statistics for the flow development. We therefore present results only for $x \leq 100$. After waiting until $t = 307$ for transients to pass, statistics were accumulated for a sample length of $T = 195$.

The turbulent boundary layer grows on the upper side of a flat plate, reaching a well-developed state with a Reynolds number of 2300 based on the displacement thickness at the trailing edge. Figure 2 shows the mean velocity at two locations, one in the developing boundary layer and one at the trailing edge, using wall units $u^+ = \langle u \rangle / u_\tau$ and $y^+ = y u_\tau / \nu$, where $u_\tau = \sqrt{\langle \tau_w \rangle / \rho}$ is the friction velocity, ρ is the density, τ_w is the shear stress on the wall and angle brackets are used to denote averages in time and over the spanwise direction z. The first profile is taken from a location sufficiently far upstream ($x = -10$) to be unaffected by the 12% increase in skin friction that occurs near the trailing edge [11]. This increase in skin friction has the effect of reducing the profile on figure 2 as the trailing edge is approached. Turbulence stresses are shown on figure 3 for the location $x = -10$ and are generally in good agreement with the incompressible simulation of Spalart [16], which was at a similar displacement thickness Reynolds number of $Re = 2000$.

The turbulent boundary layer approaching the trailing edge is resolved with grid spacings in wall units of $\Delta x^+ = 14.7$, $\Delta z^+ = 6.7$. The first point is at $y^+ = 0.75$ with ten points in $y^+ < 10$. At the trailing edge the resolution is $\Delta x^+ = 2.8$, $\Delta z^+ = 7.0$ and the first point is at $y^+ = 0.8$. Taking the streamwise location $x = 50$ as representative of the mixing layer, the local Reynolds number based on the vorticity thickness $\delta_\omega = (U_1 - U_2)/(d\langle u \rangle/dy)_{\max}$ and velocity difference $\Delta U = U_1 - U_2$ is $Re_\omega = 15900$, which is similar to the simulations of Mathew et al.[5] for a similar number of points in the spanwise and lateral directions.

3.   Results

In this section we analyse the flow just downstream of the trailing edge, focusing on instantaneous flow fields and on statistical measures of the evolving mixing layer.

3.1.   *Statistical overview*

Figure 4 shows a side view of $\partial \rho / \partial y$ for the developed flow at the location $z = 0$ at two times ($t = 488.2$ and $t = 502.2$) during the simulation. The turbulent boundary layer can be seen on the upper side of the plate. The vortical flow from this side
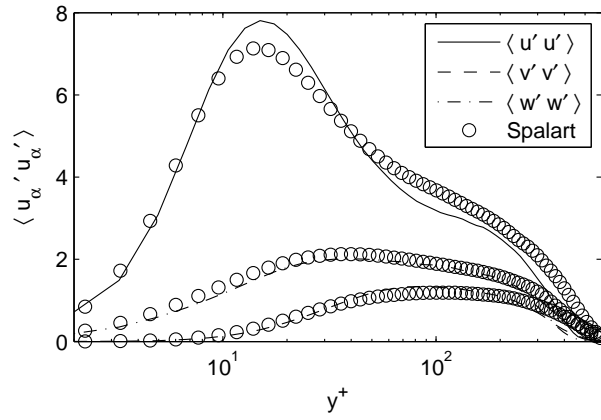
Figure 3.   Mean streamwise velocity profiles in the turbulent boundary layer upstream and at the trailing edge.
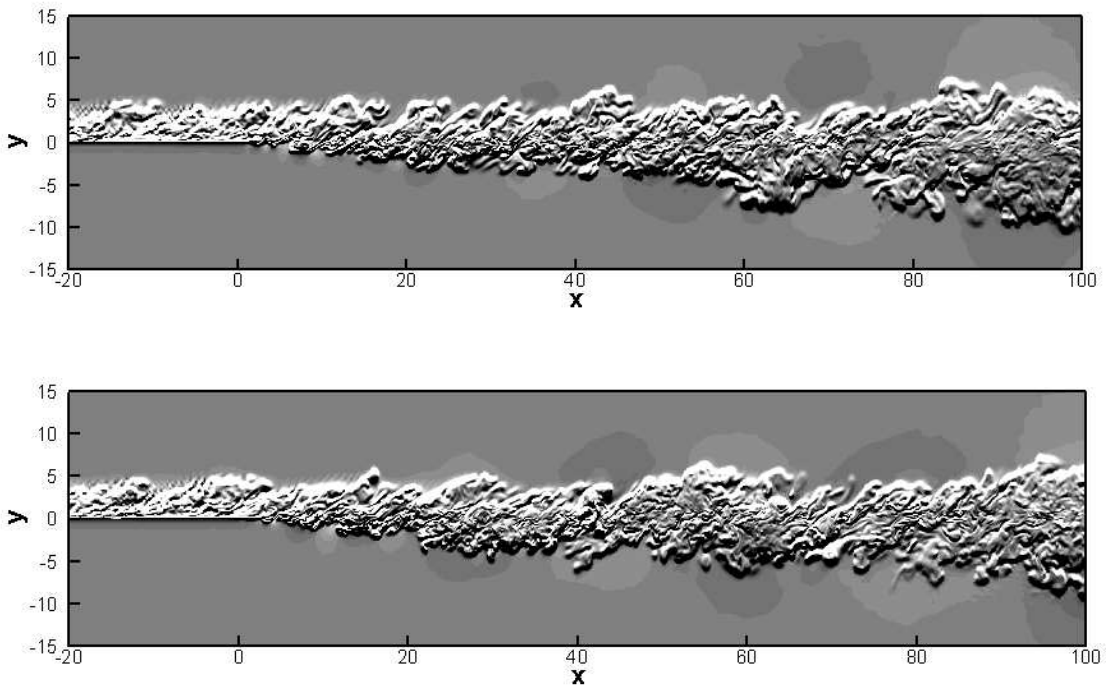

Figure 4. Contours of $d\rho/dy$, illustrating the flow structure at two times during the simulation.

of the plate is gradually entrained into the developing mixing layer, which has its origin at the trailing edge of the splitter plate. More details of the initial shear layer development are provided by figure 5, which shows two contour levels of the absolute value of the spanwise vorticity in a small region near the trailing edge. The light contour level shows a low level of vorticity and illustrates the width of the boundary layer as well as the vorticity in the laminar boundary layer on the lower side of the splitter plate. The darker contour is for a vorticity level five times the first. This shows the viscous sublayer upstream of the trailing edge and focuses attention on the internal shear layer that rolls up immediately after the end of the splitter plate. This shear layer remains distinct from the turbulent boundary layer until is has spread sufficiently (by $x \approx 50$) to entrain all the flow that was originally turbulent. A sharp turbulent/non-turbulent interface is visible on the lower side of the developing shear layer immediately downstream of the trailing edge. By
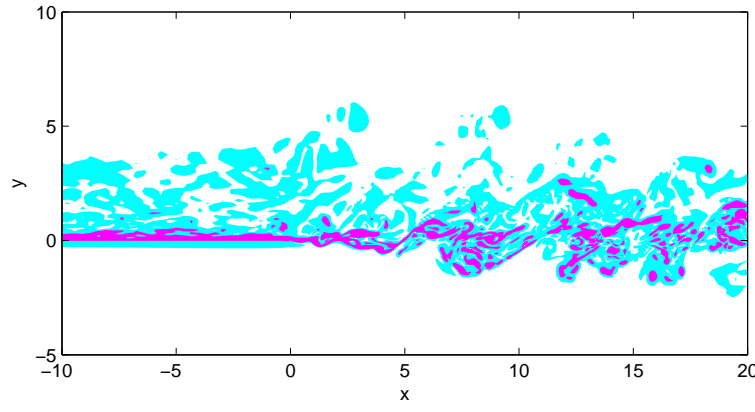
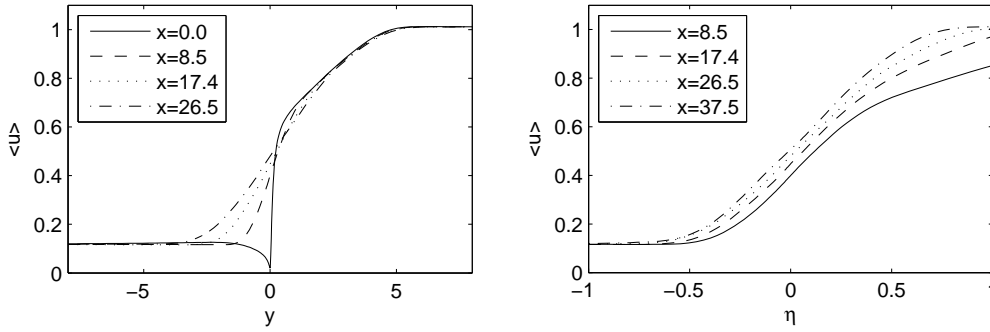Figure 5. Close-up view of spanwise vorticity near the trailing edge.

Figure 6. Velocity profiles in the initial mixing region in (a) original and (b) similarity scaling.
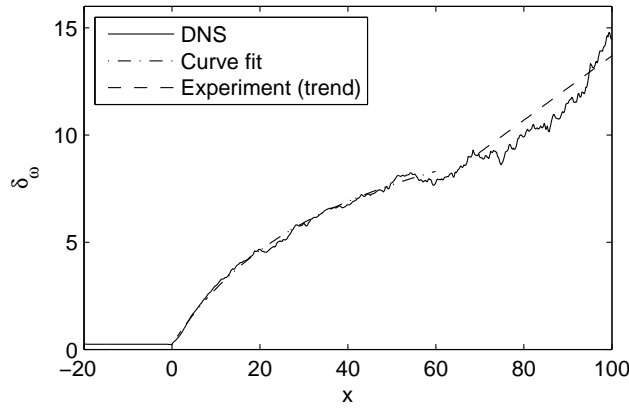

Figure 7. Thickness of the shear layer (right), including vorticity thickness, a curve fit to the initial development of the vorticity thickness and the experimental trend (dprime=0.15).

the end of figure 4 ($x = 100$), large structures are just beginning to emerge in the developed mixing layer. We caution however, that this is not proof that the current calculations capture the Brown-Roshko structures, since the domain width at $x = 100$ is only about 1.2 times the local vorticity thickness, which limits the development of structures with other orientations.

The change of the flow in the vicinity of the trailing edge is illustrated by means of velocity profiles on figure 6. Figure 6(a) shows the profiles plotted against y. Velocity profiles are shown at the trailing edge $x = 0$ and at locations in the early development of the mixing layer. It can be seen that the flow immediately behind the plate smoothes out rapidly, while it takes some distance downstream for the
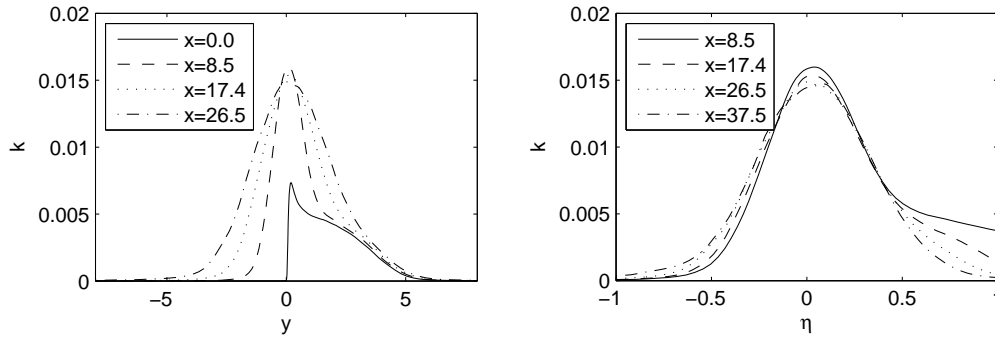
Figure 8.   Turbulence kinetic energy (k) profiles in the initial mixing region in (a) original and (b) similarity scaling.

outer region of the turbulent boundary layer to be affected. Indeed for $y > 0.3$ the profiles are essentially the same as those of the initial turbulent boundary layer. Figure 6(b) shows the profiles plotted against $\eta = y/\delta_\omega$, i.e. in a similarity coordinate using the vorticity thickness as the local length scale. Clearly the flow is not self-similar for the range of x-locations shown.

Figure 7 shows the streamwise variation of the vorticity thickness, starting from upstream of the trailing edge. The vorticity thickness can be seen to rise rapidly from its value of 0.22 at the trailing edge. Two additional curves are shown on figure 3. The first is a fit to the development of the vorticity thickness in the initial part of the flow ($0 < x < 60$), given by

$$\delta_\omega = 0.23 + \frac{0.32x}{1 + 0.023x}. \tag{1}$$

This curve fit will be used later for stability calculations. The other line shown on figure 7 is the expected growth rate of $d\delta/dx = 0.15$ based on the plots of Brown & Roshko [1] for the mixing layer parameter $\lambda = (U_1 - U_2)/(U_1 + U_2) = 0.82$. The limited statistical sample towards the end of the computational domain prevents a more detailed study of the evolution towards a self-similar state.

Figure 8(a) shows unscaled profiles of k starting from the trailing edge and illustrates a rapid change from a typical boundary-layer distribution of k at $x = 0$ to profiles with a large peak near $y = 0$. When the normal co-ordinate is scaled with δ_ω, as shown in figure 8(b) the profiles are seen to give a reasonable collapse everywhere except at the upper edge of the shear layer where the original boundary layer turbulence has not yet been entrained. The levels of k are, however, lower than those observed in temporal simulations that have attained a proper self-similar state. For example Rogers & Moser [3] and Balaras et al. [17] found peak values of $q^2/\Delta U^2$ in the range 0.06 to 0.07. This corresponds to values of k in the range 0.037 to 0.043 which are a factor of 2.5 higher than the levels seen in the present simulation. The change is not entirely due to the effective ΔU which, judging from figure 6(b), is reduced immediately downstream of the splitter plate but recovers quickly to values approaching 0.9 by $x = 37.5$.

The spatial variation of k close to the splitter plate is illustrated by means of a contour plot on figure 9. A wedge of high turbulent energy develops just downstream of the trailing edge and spreads downstream. The outer part of the turbulent boundary layer is only entrained by $x = 50$, after which the rate of growth of the mixing layer increases significantly. The initial near-collapse of k for $x < 40$ is clearly a property only of the early shear layer development. Later development shows increases of k towards the levels expected for the final self-similar state.
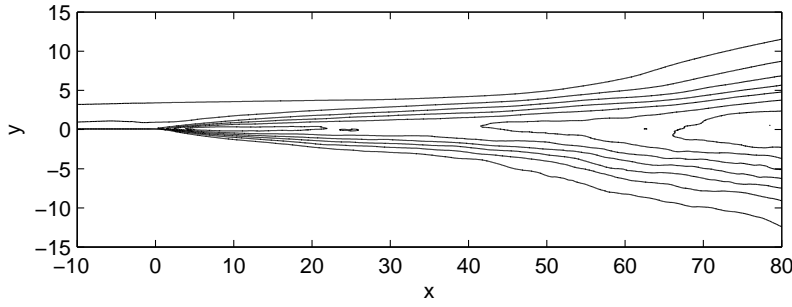
Sandham and Sandberg

Figure 9.   Contour plot of turbulence kinetic energy k (Equally spaced contours starting from 0.0025 with an increment of 0.0025).
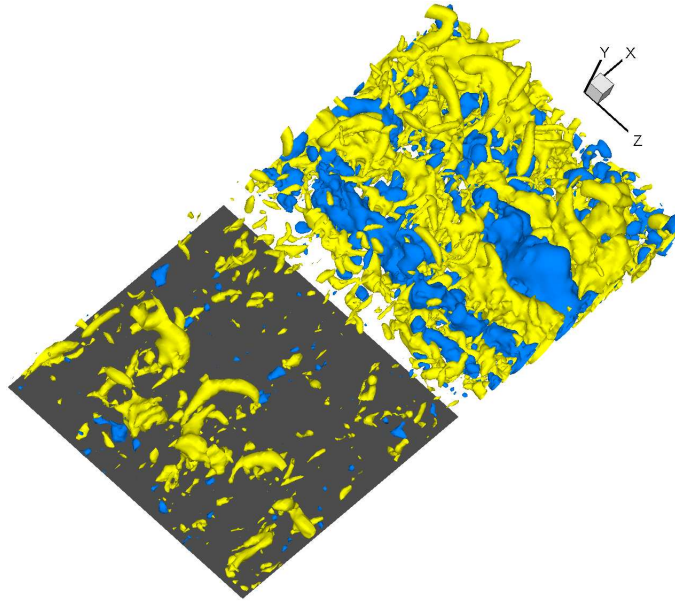
Figure 10.   Pressure fluctuations (dark surfaces are positive, light surfaces are negative), showing a close-up of the trailing edge and the early formation of spanwise-coherent structures. Flow is from lower left to upper right.

3.2.   *Flow structure immediately downstream of the splitter plate*

Figure 10 shows a close up of the trailing edge region, extending for $-19 < x < 19$. Surfaces of constant pressure perturbation, with the light surface for negative fluctuations (low pressure regions) and the dark surface for positive fluctuations (high pressure regions), reveal the presence of coherent structures. Upstream of the trailing edge we see hairpin-type structures typical of the buffer layer of a turbulent boundary layer. Within a very short distance of the trailing edge we can see evidence of partial spanwise organisation. The first high pressure zones downstream of the trailing edge are already preferentially aligned in the spanwise direction, with signs of dislocations across the span. These structures do not yet occupy the whole thickness of the turbulent shear layer and may be precursors of the later Brown-Roshko rollers, already containing a high degree of spanwise coherency.

The change in structure near the trailing edge can be quantified by considering

$$\Gamma = \frac{\langle p'_x p'_x \rangle - \langle p'_z p'_z \rangle}{\langle p'_x p'_x \rangle + \langle p'_z p'_z \rangle}, \tag{2}$$
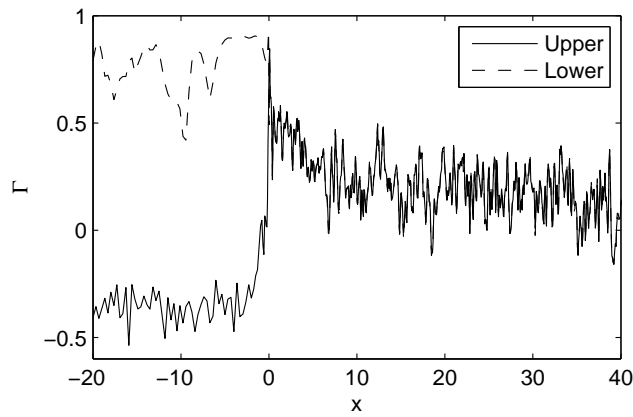
Figure 11. Structure parameter Γ on the upper and lower sides of the splitter plate, showing the rapid changes in structure near the trailing edge.
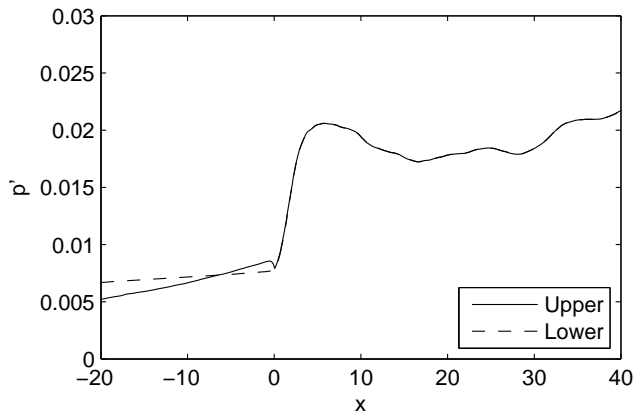

Figure 12. Root-mean-square pressure fluctuations on the upper and lower sides of the splitter plate and in the early development of the mixing layer.

where a subscript denotes differentiation. This measure is equal to 1 for purely spanwise structures and -1 for purely streamwise structures. Values of Γ were averaged over four stored flow fields at times separated by 14 time units. Figure 11 shows the development of Γ in the vicinity of the trailing edge and figure 12 shows the corresponding root mean square levels of the pressure. On the upper side of the plate (solid lines) the flow changes from a steamwise orientation of flow structure in the turbulent boundary layer ($\Gamma \approx -0.4$) to a marked spanwise orientation ($\Gamma \approx 0.5$) after the end of the plate. Thus spanwise coherency in the mixing layer develops very close to the trailing edge. The high turbulence kinetic energy developed in the mixing layer immediately after the trailing edge along with the change in structure suggests that a significant amount of turbulence energy is being pumped into the spanwise-coherent structures.

The pressure fluctuations seen on the lower side of the plate upstream of the trailing edge on figures 11 and 12 are long wavelength acoustic waves propagating upstream. These are oriented in the spanwise direction due to the scattering characteristics of the trailing edge. The present results may be compared with the wake aeroacoustic calculations of Sandberg & Sandham [11] which showed that acoustic radiation from a sharp trailing edge is predominantly two-dimensional. The high value of Γ reached on the lower surface of the plate is important evidence that the splitter plate trailing edge serves to organise at least some part of the flow into a spanwise-coherent form.
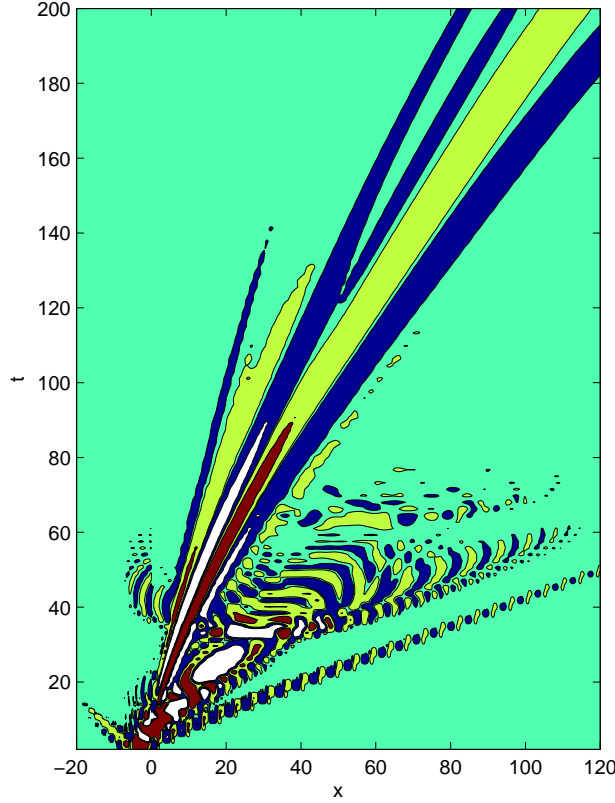
Figure 13. Impulse response of the time-averaged flow. Contours of pressure along the centreline on x-t axes show the development in space and time of the wavepacket arising from the initial perturbation.

4.   Assessment of mechanisms

In this section we test two of the mechanisms discussed in the introduction as being possible causes of enhanced two dimensionality in the mixing layer downstream of a trailing edge.

4.1.   *Test for the presence of a global instability*

A global mode (Huerre & Monkewitz [18]) may be defined using the ansatz

$$\phi' = \hat{\phi}(x, y) \exp(i\beta z + \sigma t), \tag{3}$$

where ϕ' is a perturbation in a flow variable, $\hat{\phi}$ is the mode shape, β is a spanwise wavenumber and σ is a growth factor. If the real part of σ is positive the flow is globally unstable. In this section we use a numerical approach to test for the presence of a global instability. The method tests the impulse response of the flow, as in the method of discriminating absolute and convective instabilities in parallel shear flows (see [18] for a review). In the numerical approach the time-averaged (non-parallel) mixing layer is used as the base flow, upon which the evolution of small disturbances is computed. Practically this is achieved by computing the imbalance in the instantaneous Navier-Stokes equations by running one Runge-Kutta substep with the time averaged conservative variables. The imbalance for the momentum equations is the Reynolds stress term, while the imbalance for the

energy equation involves Reynolds stress and heat conduction terms. The imbalance is then canceled by applying a forcing term to the Navier-Stokes equations such that when the equations are integrated forward in time the base flow is maintained as a fixed reference flow. After checking that the base flow is maintained it is then possible to add small perturbations and check whether these grow or decay. The same method has been used by Touber & Sandham [19] to compute the global mode of a shock-wave/boundary-layer interaction problem. The method makes use of an existing (validated) Navier-Stokes solver but is limited in comparison with global-mode analyses (see e.g. Theofilis [20]), in that it can only deliver the most unstable (or least damped) global mode. Also, no attempt is made to account for the effect of turbulence on the developing instability mode.

For the present calculations an impulse was added to the flow just upstream of the trailing edge with an amplitude of 10^{-8} and then the integration was carried forward in time. Figure 13 shows contours of pressure along $y = 0$ on an $x - t$ diagram. The initial impulse was provided just upstream of the trailing edge at $t = 0$. Both downstream and (weaker) upstream-propagating sound waves can be observed starting from the initial perturbation. After transient effects have dissipated (by about $t = 80$) we can see a linear wave packet that spreads as it moves downstream. The slope decreases with increasing time, since the convection speed rises. This can be seen from figure 6(b) where the local velocity at the inflection point increases by approximately 25% from $x = 8.5$ to $x = 37.5$. The left boundary of the wave packet envelope is clearly convecting downstream and the conclusion of this analysis is that the flow is convectively unstable and there are no unstable global modes. A simple method to account for the effect of turbulence on the instability modes would be to add an eddy viscosity. This would act to reduce the growth rates of disturbances, but is unlikely to lead to any change in the global stability character. Although no evidence for an unstable global mode has been found, the results of this section do not preclude the presence of a marginally stable global mode that may be excited by upstream disturbances and in the process change the flow structure.

4.2. *Convective growth model*

In the absence of an unstable global mode, it is necessary to check whether a convective growth of disturbances, which is preferentially two-dimensional from linear stability analysis, is sufficient to explain the main structures seen in figure 10 and the tendency to spanwise coherency seen in Γ (figure 11). There is known to be a strong connection between shear layer growth rate and growth rates obtained from linear stability theory (see e.g. [21] [22] [23]). In this subsection we construct a model of the growth of instabilities to test whether it is plausible for the observed structural changes to emerge from convective amplification alone.

With a parallel flow assumption the convective model can be represented by normal modes

$$\phi' = \hat{\phi}(y) \exp(i(\alpha x + \beta z - \omega t), \tag{4}$$

where the frequency ω and the spanwise wavenumber β are real and the streamwise wavenumber α is complex. The spatial growth rate is given by $-\alpha_i$ and the wave angle by $\theta = \tan^{-1}(\beta/\alpha_r)$. With local scaling using δ_ω and U_1, Figure 14 shows the growth rate as a function of frequency for wave angles of θ equal to 0°, 30° and 60°, using the linear stability solver from [22]. It can be seen that the local growth rates and range of unstable frequencies only reduce significantly for $\theta > 30°$. To find
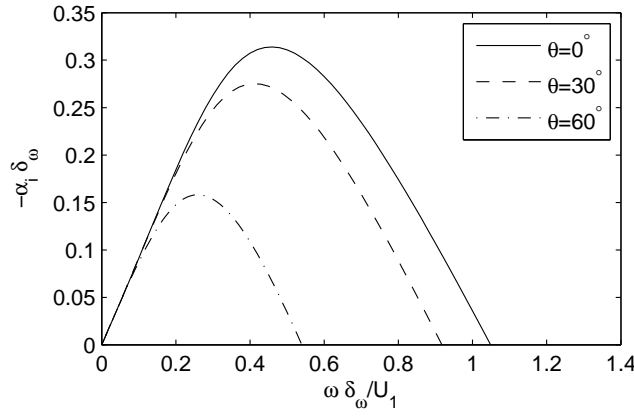
Sandham and Sandberg

Figure 14.   Variation of spatial growth rate with frequency from linear stability theory for $U_1 = 1, U_2 = 0.1$. Stability curves are plotted for three wave angles θ.
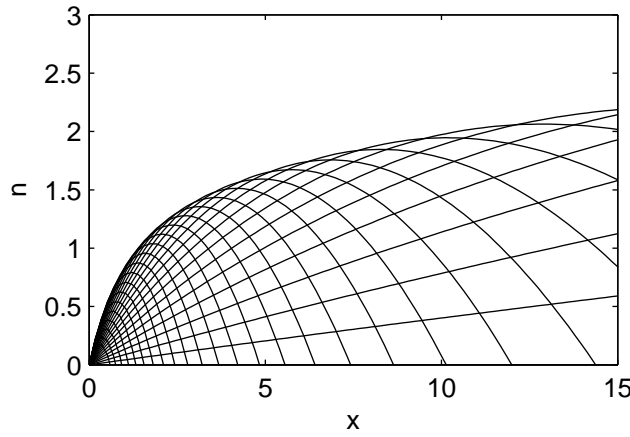

Figure 15. Variation of growth factor downstream of splitter plate for disturbances at $\theta = 0°$.

the overall amplification for a particular frequency we define and growth factor as $n = \ln(A/A_0)$ where A is an amplitude and A_0 is the amplitude at some reference location. Curves for the variation of n with x are found by integrating

$$\frac{dn}{dx} = -\alpha_i, \tag{5}$$

using splined data from figure 14 together with the curve fit to the initial variation in δ_ω taken from equation (1). Results for the $n-$factor variation with x are shown on figure 15 for 30 distinct frequencies. The largest n-factor at any given x defines the envelope of the most amplified waves relative to $x = 0$. The values of the peak n-factor are not large in comparison to the typical values of $n = 9$ used for transition predictions. The amplification factors at $x = 5$ are $n = 1.53$ for $\theta = 0°$, $n = 1.34$ for $\theta = 30°$ and $n = 0.77$ for $\theta = 60°$.

To see whether this sort of amplitude growth may be significant we consider a flow structure given by a superposition of waves with different obliqueness. A two-dimensional $x - z$ field (for example of pressure p) is generated by adding six waves together

$$p = \sum_{k=1}^{6} a_k \exp(\alpha_k x + \beta_k z + \phi_k). \tag{6}$$

Table 1.   Data for mode superposition model.

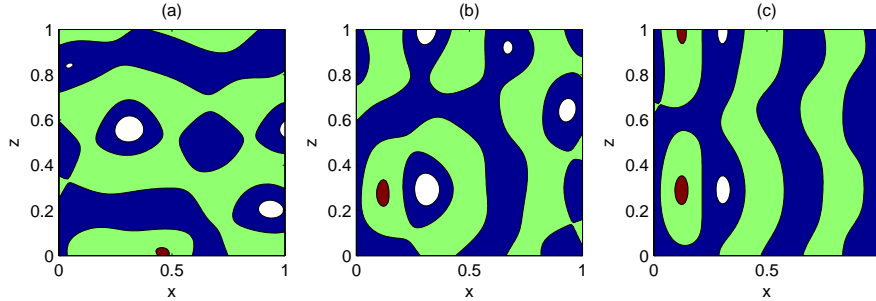| k	α_k	β_k	$\theta_k(\deg)$	a_k	n_k
1	6π	0	0	1.0	1.53
2	$3\sqrt{3}\pi$	3π	30	1.0	1.34
3	3π	$3\sqrt{3}\pi$	60	1.0	0.77
4	0	6π	90	2.1	0.0
5	3π	$-3\sqrt{3}\pi$	120	1.0	0.77
6	$3\sqrt{3}\pi$	-3π	150	1.0	1.34

Figure 16.   Result of the mode superposition model, comparing (a) structure with $\Gamma = -0.42$, representing the flow upstream of the trailing edge (b) a flow field just downstream of the trailing edge after selective amplification by the factors in Table 1, in which $\Gamma = 0.46$, and (c) a flow further downstream with $\Gamma = 0.77$.

The values of the amplitude a_k and the wavenumbers α_k and β_k are shown on Table 1, together with the wave angle θ_k. The phase ϕ_k is a random variable. The amplitude a_4 is increased so that initially $\Gamma = -0.42$, which is representative of the flow upstream of the trailing edge, as seen in figure 11. The resulting flow structure (for one set of random phases) is shown on figure 16(a). It can be seen that the flow structures indeed appear more streamwise-oriented, as expected for such a value of Γ.

The amplitudes are then changed by factors reflecting the effect of convective growth. For example a wave $k = 1$ with $\theta_1 = 0°$ is assumed to grow by a growth factor of $n_1 = 1.53$, while waves with $\theta = 90°$ are assumed to be neutral ($n_4 = 0$). The resulting flow after such a convective growth process is shown on figure 16(b), where Γ has increased to $+0.46$. The ease with which the value of Γ is matched suggests that growth in amplitude by a factor of 5 for two-dimensional waves is sufficient to give the change in structure seen at the end of the plate. One discrepancy is that the growth seen in figure 8 is very rapid, starting from upstream of the trailing edge, rather than a gradual growth as on the $n-$factor plot (figure 15). This may be due to the upstream influence of the low pressure vortex cores that form very close to the trailing edge. Nevertheless it does appear that the convective model provides a plausible explanation for the structural changes in the turbulence occurring very close to the trailing edge.

The convective model has been extended downstream, using a composite equation for the development of the vorticity thickness, using equation (1) up to $x = 60$ and thereafter using

$$\delta_\omega = 0.15(x - 4.685). \tag{7}$$

A plot of the resulting n-factor is shown on figure 17 illustrating how the curves reach a plateau downstream. The largest n-factors for disturbance angles of $0°$, $30°$ and $60°$ are 3.96, 3.47 and 2.00 respectively. Substituting these values into the mode superposition model gives an increased value $\Gamma = 0.77$ for the structural parameter. Thus it appears that the same convective model, extended downstream,
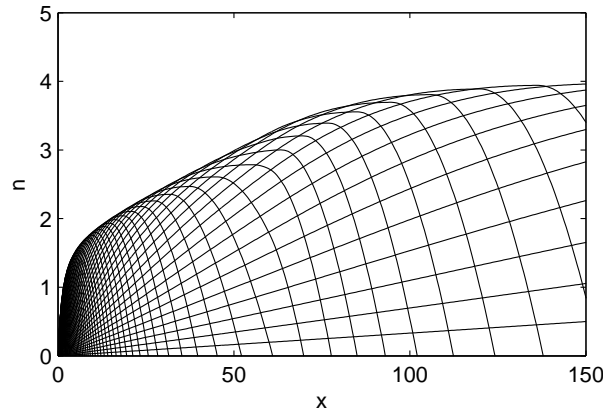
Figure 17. Variation of growth factor downstream of splitter plate for disturbances at $\theta = 0°$.

predicts an increased level of two-dimensionality in the developed mixing layer ($x > 150$). The relative values of the final n-factors for waves of different angles are not highly dependent on the initial development of the vorticity thickness plot, since calculations of a mixing layer developing from $x = 5$ and following the variation given by equation (7) gave essentially the same results.

5.   Conclusion

Direct numerical simulations have been conducted of a spatially developing mixing layer at a high velocity ratio, including the trailing edge in the computational domain. A turbulent boundary layer on the upstream plate undergoes a rapid change in structure as it passes the trailing edge. Associated with this is the development of a region of high turbulence kinetic energy and a change from streamwise- to spanwise-oriented flow structures. The region near the trailing edge appears to provide rapid amplification of a broad band of preferentially spanwise-oriented structures. In the present simulations this leads to the generation of structures with a range of small angles of obliqueness, but not straightaway to large coherent spanwise rollers.

With respect to the origin of the two-dimensional structure in the mixing layer, the present study has ruled out the influence of a global mode at the trailing edge for the case where the splitter plate is infinitely thin. Taken together with previous results, there appears to be a critical thickness beyond which the flow would be globally unstable, resulting in a strong resonant behaviour in the near wake of the trailing edge. Whether previous experiments were in the thin splitter plate limit, as studied here, or were affected by trailing edge thickness (and/or included angle) is something that could be clarified by further simulations.

A quantitative explanation for enhanced two-dimensionality seen in the simulation has been provided by a convective instability model. It has been demonstrated that this model is consistent with the observed change in flow structure near the trailing edge of the splitter plate. The same model, extended downstream, predicts an increased level of two-dimensionality in the fully-developed mixing layer. The success of the convective model in the current mixing layer application is further evidence for the important role played by instability waves in this class of shear flows.

The present study provides partial support for a mechanism of receptivity at the trailing edge. The presence of a splitter plate appears not to be sufficient by itself to cause highly spanwise-coherent structures in the early development

of the mixing layer. However, if the sound waves generated at the trailing edge are closely two-dimensional, particularly at lower frequencies, this could influence large structures, for example by reflecting from the upper and lower walls in the experiment and triggering preferentially-two-dimensional vortical modes when the reflected waves pass the trailing edge. Such a mechanism could explain why the present simulation did not reproduce the high levels of spanwise-coherence that were seen in experiments from very early in the mixing layer development.

6.   Acknowledgements

References

[1] G.L. Brown and A. Roshko, *On density effects and large structure in turbulent mixing layers*, J. Fluid Mech. 64 (1974), pp. 775–816.
[2] J.E. Broadwell and M.G. Mungal, *Large-scale structures and molecular mixing*, Phys. Fluids A 3(5) (1991), pp. 1193–1206.
[3] M.M. Rogers and R.D. Moser, *Direct simulation of a self-similar turbulent mixing layer*, Phys. Fluids 6(2) (1994), pp. 902-923.
[4] C.-M. Ho and P. Huerre, *Perturbed free shear layers*, Ann. Rev. Fluid Mech. 16 (1984), pp. 365–424.
[5] J. Mathew, I. Mahle and R. Friedrich, *Effects of compressibility and heat release on entrainment processes in mixing layers*, Journal of Turbulence 9(14) (2008), pp. 1–12.
[6] M. Tanahashi, Y. Wang, T. Fujisawa, M. Sato, K. Chinda and T. Miyauchi, *Fractal geometry and mixing transition in turbulent mixing layers*, Fifth International Symposium on Turbulence and Shear Flow Phenomena, TU München, Garching, Germany, Aug 27-29 2007.
[7] R.D. Mehta, *Effect of velocity ratio on plane mixing layer development - influence of the splitter plate wake*, Experiments in Fluids 10(4) (1991), pp. 194–204.
[8] L.S. Lee and P.J. Morris, *Absolute instability in a supersonic shear layer and mixing control*, J. Propulsion and Power 13(6) (1997), pp. 763–767.
[9] M.F. Barone and S.K. Lele, *Receptivity of the compressible mixing layer*, J. Fluid Mech. 540 (2005), pp. 301–335.
[10] S. Laizet and E. Lamballais, *Simulation numérique directe de l'influence de la forme aval d'une séparatrice sur une couche de mélange*, Comptes Rendus Mecanique 334 (2006), pp. 454–460.
[11] R.D. Sandberg and N.D. Sandham, *Direct numerical simulation of turbulent flow past a trailing edge and the associated noise generation*, J. Fluid Mech. 596 (2008), pp. 353–385.
[12] H.C. Yee, N.D. Sandham and M.J. Djomeri, *Low-dissipative high-order shock-capturing methods using characteristic-based filters*, J. Comp. Phys. 150(1) (1999), pp. 199–238.
[13] N.D. Sandham, Q. Li and H.C. Yee, *Entropy splitting for high-order simulation of compressible turbulence*, J. Comp. Phys. 178(2) (2003), pp. 307–322.
[14] L.E. Jones, R.D. Sandberg and N.D. Sandham, *Direct numerical simulation of forced and unforced separation bubbles on an airfoil at incidence*, J. Fluid Mech. 602 (2008), pp. 175–207.
[15] R.D. Sandberg and N.D. Sandham, *Nonreflecting zonal characteristic boundary condition for direct numerical simulation of aerodynamic sound*, AIAA Journal 44(2) (2006), pp. 402–405.
[16] P.R. Spalart, *Direct simulation of a turbulent boundary-layer up to $Re_\theta = 1410$* J. Fluid Mech. 187 (1988), pp. 61-98.
[17] E. Balaras, U. Piomelli and J.M. Wallace, *Self-similar states in turbulent mixing layers*, J. Fluid Mech. 446 (2001), pp. 1–24.
[18] P. Huerre and P.A. Monkewitz, *Local and global instabilities in spatially developing flows*, Ann. Rev. Fluid Mech. 22 (1990), pp. 473–537.
[19] E. Touber and N.D. Sandham, *Oblique shock impinging on a turbulent boundary layer: low-frequency mechanisms*, AIAA paper 2008-4170 (2008) pp. 1–27.
[20] V. Theofilis, *Advances in global linear stability analysis of nonparallel and three-dimensional flows*, Progress in Aerospace Sciences 39(4) (2003), pp. 249–315.
[21] M.Gaster, E. Kit and I. Wygnanski, *Large-scale structures in a forced turbulent mixing layer*, J. Fluid Mech. 150 (1985), pp. 23–39.
[22] N.D. Sandham and W.C. Reynolds, *Compressible mixing layer: linear theory and direct simulation*, AIAA Journal 28(4) (1990), pp. 618–624.
[23] P.J. Morris, M.G. Giridharan and G.M. Lilley, *On the turbulent mixing of compresible free shear layers*, Proc. R. Soc. Lond. A 431 (1990), pp. 219–243.